Steel and Composite Structures, *Vol. 17*, *No. 5* (*2014*) *687-704*
DOI: http://dx.doi.org/10.12989/scs.2014.17.5.687

Effect of post weld treatment on cracking behaviors of beam-column connections in steel bridge piers

Liang-Jiu Jia [1a], Hanbin Ge [*2] and Toshimitsu Suzuki [3b]

[1] *Advanced Research Center for Natural Disaster Risk Reduction*, *Meijo University*, *1-501 Shiogamaguchi*, *Tenpaku-ku*, *Nagoya*, *468-8502*, *Japan*
[2] *Deptartment of Civil Engineering*, *Meijo University*, *1-501 Shiogamaguchi*, *Tenpaku-ku*, *Nagoya*, *468-8502*, *Japan*
[3] *Hiroshima Machinery Works*, *Mitubishi Heavy Industries*, *Ltd.*, *5-1 Ebaokimachi*, *Naka-ku*, *Hiroshima*, *730-8642*, *Japan*

(*Received January 14*, *2014*, *Revised April 16*, *2014*, *Accepted April 17*, *2014*)

Abstract. A great number of moment-resisting steel structures collapsed due to ductile crack initiation at welded beam-column connections, followed by explosive brittle fracture in the Kobe (Hyogoken-Nanbu) earthquake in 1995. A series of experimental and numerical studies on cracking behaviors of beam-column connections in steel bridge piers were carried out by the authors' team. This paper aims to study the effect of post weld treatment on cracking behaviors of the connections during a strong earthquake event. Experiments of three specimens with different weld finishes, i.e., as-welded, R-finish, and burr grinding, were conducted. The experimental results indicate that the instants of ductile crack initiation are greatly delayed for the specimens with R-finish and burr grinding finishes compared with the as-welded one. The strain concentration effect in the connection is also greatly reduced in the specimens with post weld treatment compared with the as-welded one, which was also verified in the tests.

Keywords: ductile fracture; post weld treatment; burr grinding; R-finish; beam-column connection; steel bridge pier

1. Introduction

During strong earthquakes, welded beam-column connections in moment-resisting steel structures are susceptible to brittle fracture triggered by ductile crack initiation at the welds (Kuwamura 1997), which was first observed in a large number of steel building structures during the Northridge earthquake in 1994 (AIJ 1995, Kuwamura Lab. 1995, Nakashima *et al*. 1998) and the Kobe (Hyogoken-Nanbu) earthquake in 1995 (Mahin 1998, O'Sullivan *et al*. 1998). A similar cracking process was also found at welded beam-column connections in steel moment resisting frame (SMRF) bridge piers (Miki and Sasaki 2005, Usami and Ge 2009). It was pointed out that

∗Corresponding author, Professor, E-mail: gehanbin@meijo-u.ac.jp
[a] Ph.D., E-mail: LJ_JIA@hotmail.com
[b] Dr. Eng., E-mail: toshimitsu_suzuki@mbe.mhi.co.jp

http://www.techno-press.org/?journal=scs&subpage=8 ISSN: 1229-9367 (Print), 1598-6233 (Online)

the brittle fracture during the Kobe earthquake could be divided into three critical steps, i.e., ductile crack initiation at locations with strain concentration, ductile crack propagation, and progressive failure due to brittle fracture (Kuwamura 1997, Kuwamura and Yamamoto 1997). The failure process was found to be similar to those occurred in beam-column connections in steel piers during the Kobe earthquake (Miki and Sasaki 2005, Usami and Ge 2009). Brittle fracture was also observed in a rectangular steel column at the height of concrete-fill, and a cast steel pier (Bruneau *et al*. 1996). Therefore, it is of great importance to study the ductile cracking behaviors preceding the brittle fracture in steel bridge piers.

After the two earthquakes, comprehensive studies on the mechanism of brittle fracture during strong earthquakes and new measurements to avoid brittle fracture were conducted by both Japanese and U.S. researchers (e.g., EI-Tawil *et al*. 2000, Schafer *et al*. 2000, Stojadinović *et al*. 2000, Mao *et al*. 2001, Ricles *et al*. 2002, Kuwamura 2003, Kuwamura *et al*. 2003, Qian *et al*. 2005, Roeder *et al*. 2005). A new Federal Emergency Management Agency (FEMA) recommended design criterion aiming to produce a more ductile seismic design of welded SMRF buildings was proposed after the Northridge earthquake (FEMA-350 2000). An interim guideline to prevent brittle fracture at the welds of the connections in SMRF buildings was also published by the Building Center of Japan (2003). Extensive research on brittle fracture of SMRF buildings has been conducted, while limited studies on brittle fracture of SMRF bridge piers have been conducted since the two earthquakes.

On the other hand, post weld treatments were found to be effective in increasing the fatigue life of welded structures in high cycle and medium cycle regimes (e.g., Haagensen and Maddox 2001, Pedersen *et al*. 2010, Kirkhope *et al*. 1999a, b, Mashiri *et al*. 2001, Iwashita and Azuma 2012, Qian *et al*. 2013). Common weld treatment methods can be divided into two categories: weld geometry improvement methods, and residual compressive stress methods. The former improves the crack-like geometry at the welds, and reduces the strain concentration. The latter introduces compressive pre-stress into the weld toes to delay the occurrence of cracking mainly due to tensile stress. The former includes grinding methods such as burr grinding (BG); re-melting methods such as tungsten inert gas (TIG) dressing; and weld profile control methods etc. To improve the fatigue life of the welded beam-column connections in steel bridge piers, BG finish at the weld toes, and large-scale fillets at the beam-web-to-column-web joints were required in practical constructions for newly built highway bridges recently (Nagoya Expressway Public Corporation 2004,

Fig. 1 Beam-column connections in steel piers with very small fillet radius

Metropolitan Expressway Company Limited 2008). However, the effect of post weld treatment on ductile cracking life of welded beam-column connections in steel bridge piers has seldom been found in the literature.

A series of experimental and numerical studies on ductile crack initiation of cantilever piers and beam-column connections have been carried out by the authors' team (Ge and Luo 2011, Ge and Kang 2012, Kang and Ge 2013, Luo *et al*. 2012, Ge *et al*. 2013). This paper aims to experimentally study the effect of post weld treatments on ductile cracking behaviors of the beam-column connections in steel bridge piers with three different weld finishes: as-welded (AW), R-finish, and BG, under a strong earthquake event. Three thick-walled beam-column connections with the same global geometrical and structural parameters were tested under cyclic incremental loading. The experimental results indicate that the ductile cracking initiation life was greatly improved for both of the two specimens with post weld treatments. The weld finishes were also found to be effective in reducing the strain concentration effect near the weld toes at the beam-flange-to-column-flange joints.

2. Experimental program

2.1 Introduction of the adopted two weld treatment methods

In practice, there are no weld treatments to the beam-column connections for many steel bridge piers constructed several decades ago, and weld toe burr grinding is commonly applied to the ones built recently as illustrated in Fig. 1. Herein, only the methods commonly employed in steel bridges are briefly reviewed, e.g., the BG method, and an improved profile weld method (American Welding Society D1.1 1996) which is termed R-finish in this paper. The details and actual configurations of the three finishes are shown in Fig. 2. The BG finish at the weld toes is to remove the surface defects, and make a smooth transition between the base metal and the weld beads, which can thus improve the strain concentration effect due to the original irregular sharp corners. The detailed procedure for performing weld toe BG can refer to the recommendations of the International Institute of Welding (IIW) (Haagensen and Maddox 2001). Though a small smooth notch remains at the weld toes after the BG finish, the strain concentration effect is still reduced compared with the as-welded connections. On the other hand, the R-finish method recommended by the AWS is to obtain a smooth transition by controlling the overall profile of the weld. By application of the R-finish, the strain concentration can be moved to a location with a lower strain concentration factor, which can improve the fatigue life of welded structures (Kirkhope *et al*. 1999a). The R-finish method will reduce the size of the weld throat, which may affect the static strength in some cases, and special attentions should be paid to control the throat thickness, especially for ductile cracking which is closely related with the static strength.

2.2 Configuration of specimens

Three full-penetration welded specimens of unstiffened beam-column connections were manufactured to simulate the welded connections in the thick-walled SMRF bridge piers. The configuration of the specimens is illustrated in Fig. 2, and measured dimensions and structural parameters of the specimens are listed in Table 1, where the numbering of the specimen "SOO-*a*-15-AW(R, BG)-VC" denotes: S = steel, OO = the value of the width-to-thickness ratio parameter, R_f, multiplied by 100, *a* = incomplete penetration depth, 15 = designed radius of the

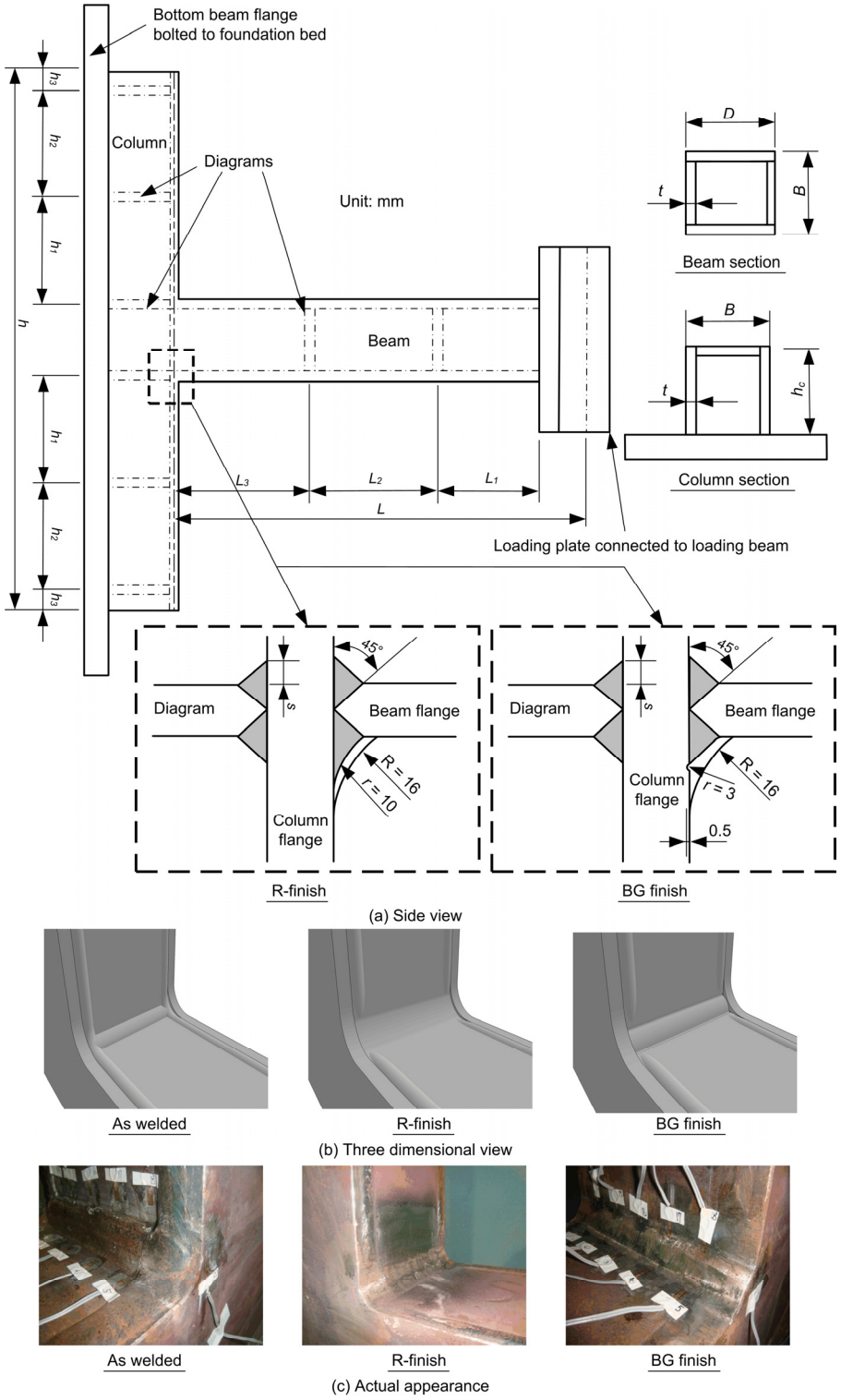

Fig. 2 Configuration of specimens

Table 1 Measured dimensions and structural parameters of the specimens

Specimens	Geometrical dimensions (mm)														Structural parameters			
	h	h_1	h_2	h_3	h_c	L	L_1	L_2	L_3	B	D	t	R	a	R_f	$\bar{\lambda}$	H_y (kN)	δ_y (mm)
S30-0-15-AW-VC	857	168	164	16	163	769	225	225	225	175	173	11.77	16	0	0.31	0.31	201	4.71
S30-0-15-R-VC	858	168	164	16	164	769	225	225	225	175	174	11.77	16	0	0.31	0.31	200	4.67
S30-0-15-BG-VC	858	168	164	16	164	769	225	225	225	175	174	11.77	16	0	0.31	0.31	200	4.68

*Notes:

(1) Notation of test specimens, e.g., SOO-*a*-15-AW(R, BG)-VC, S = steel; OO = value of the width-to-thickness ratio parameter, R_f, multiplied by 100; a = incomplete penetration depth; AW = as-welded, R = R-finish, and BG = burr grinding; VC = variable amplitude cyclic loading.

(2) h = column height; L = beam length; B = flange width of beam and column; D = web width of beam; h_c = web width of column; t = thickness; R = curvature radius of the fillet; $\bar{\lambda}$ = slenderness ratio parameter; H_y = yield strength of lateral load; δ_y = yield displacement of lateral load.

Table 2 Mechanical properties and chemical compositions of welding wires

Mechanical properties				Chemical compositions (%)					
Yield stress (N/mm^2)	Tensile strength (N/mm^2)	Elongation (%)	Charpy impact energy (J)	C	S	Mn	P	S	Cu
613	648	25	83 (0°C)	0.05	0.46	1.74	0.014	0.005	0.32

Table 3 Coupon test results of base metal

σ_y (MPa)	ε_y (%)	σ_u (MPa)	ε_f (%)	ν	E (GPa)	E_{st} (GPa)	ε_{st} (%)
384	0.182	532	25.7	0.285	211	4.6	2.21

*Note: σ_y = yield stress, ε_y = yield strain, σ_u = tensile strength, ε_f = uniform strain at fracture, ν = Poisson's ratio, E = Young's modulus, E_{st} = strain hardening modulus, ε_{st} = strain at initiation of strain hardening

fillet at the beam-flange-to-column-flange joint, AW = as welded, R = R-finish, BG = weld toe burr grinding, and VC = variable amplitude cyclic loading. The base metal of the columns and beams was made of SM490YA, which is widely applied to practical construction of steel bridges in Japan. Both the columns and the beams were of welded rectangular sections, and the wall thickness was designed as 12 mm considering the capacity of the loading device. The weld metal YFW-C50DM was employed, and its mechanical properties and chemical compositions are given in Table 2. The mechanical properties of the base metal, obtained from average values of three coupon tests, are given in Table 3, where the average fracture strain, ε_f, was calculated from the measured elongation within a gage length after fracture of the coupons. The secant modulus, ε_{st}, was obtained using the least square method based on the stress-strain data in the strain hardening ranges until necking initiates.

For the specimen with BG finish, a grinding depth of 0.5 mm was selected, which is the required minimum size for the BG finish. The resulting root radius of the BG finish is 3 mm,

which is the required minimum size by the IIW recommendations (Haagensen and Maddox 2001). For the R-finish, a fillet radius of 10 mm was selected considering the weld throat thickness and manufacturing conditions. The weld surfaces of the specimen with R-finish are smooth and clear, which facilitate the observation of crack initiation and propagation during experiments. Besides, a small fillet with a radius of 15 mm was designed at the beam-web-to-column-web joint to simulate the actual configurations of steel bridges with small fillets as illustrated in Fig. 1. In recently constructed bridges, a fillet radius ranging from 100 mm to 20% of the beam height is employed to obtain a smooth stress transition at the beam-column connections. Since this paper is focused on the effect of post weld treatment, the small fillet size was selected. The fillet radius of 15 mm is also the minimum value for the current manufacturing technologies. Three diagrams were designed inside the beam members with intervals of L_1, L_2, and L_3, from the right ends of the beams. Likewise, six diagrams were also added inside the column members. The left column flange was replaced by a thick plate, which was to simplify the boundary conditions of the beam-column connections. A loading plate was welded to the right end of the beam to connect with a loading beam using high strength bolts. Both the assembling and welding procedure of the plates of the beam-column connections were the same as those employed in practice, except that two backing plates were employed at one of beam-web-to-column-flange joints and beam-flange-to-beam-web joints, which are required by the welding workmanship due to the poor welding accessibility and limited working space. To exclude the effect of the backing plates, the ends of the backing plates close to the beam-web-to-column-web joints were cut to avoid intersections of welds.

A small width-to-thickness ratio parameter, R_f, was selected to avoid the influence of local buckling of the beams, which may result in decrease in the loads and make the problem more complicated. Therefore, a width-to-thickness ratio parameter, R_f, of 0.3 defined in Eq. (1) was determined.

$$R_f = \frac{b}{t}\sqrt{\frac{12(1-\nu^2)}{\pi^2 \cdot 4n^2}}\sqrt{\frac{\sigma_y}{E}} \tag{1}$$

where b = width of beam flange, t = thickness of beam flange, σ_y = yield stress, E = Young's modulus, v = Poisson's ratio, and n = number of sub-panels. The value of n should be 1 since the section is unstiffened.

The slenderness ratio parameter, $\overline{\lambda}$, of 0.31 defined according to Eq. (2) were designed to avoid premature global instability of the beams during loading.

$$\overline{\lambda} = \frac{2L}{r}\frac{1}{\pi}\sqrt{\frac{\sigma_y}{E}} \tag{2}$$

where L = beam length, and r = radius of gyration.

2.3 Test setup and loading history

Experiments on the specimens were conducted using a self-balanced steel reaction frame and two horizontal actuators each with a force capacity of ± 1000 kN, and a displacement capacity of ± 500 mm, as illustrated in Fig. 3. A moving loading beam and a pin-connected loading beam were employed. The specimen was rotated by 90 degrees to accommodate the loading frame, and the

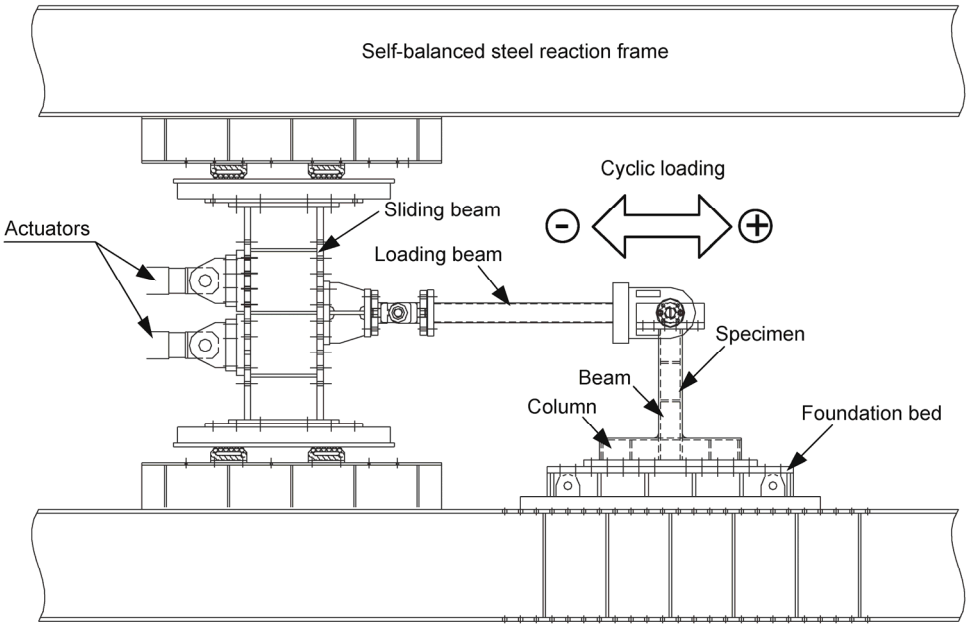

Fig. 3 Test setup

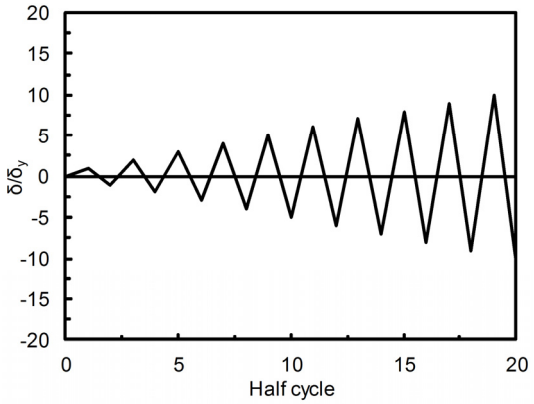

Fig. 4 Loading history

bottom column flange of the specimen was connected to a foundation bed using high strength bolts. Displacement transducers were employed to measure the horizontal displacements at the upper beam end and the two column ends. The stroke of the actuators and the vertical displacements of the column were also measured to obtain the small rotation of the whole specimen. The net horizontal displacement at the upper beam end was employed for the controlling of all the tests. An incremental loading history with one cycle per displacement amplitude as illustrated in Fig. 4 was employed in this study. The four corners of the connections were numbered as illustrated in Fig. 5.

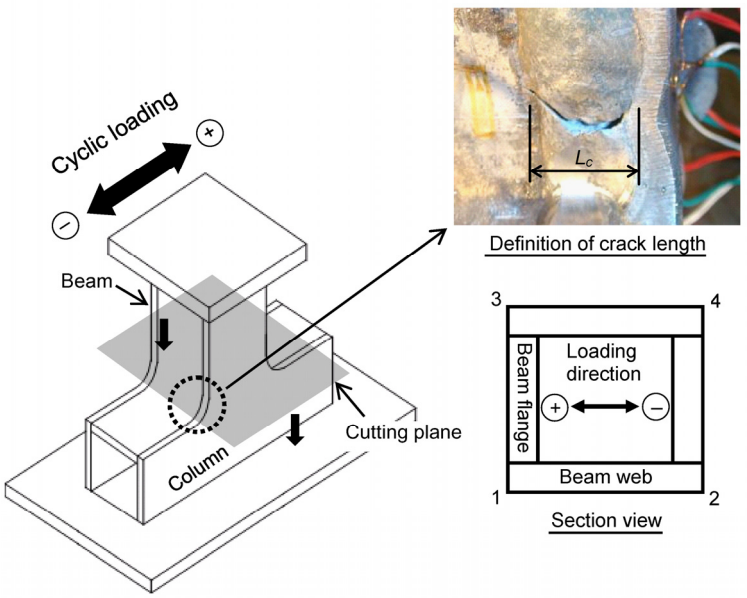

Fig. 5 Numbering of the corners and definition of crack length

3. Experimental results

3.1 Definition of cracking initiation

Definition of crack initiation is of great importance for this study. The instant at crack initiation is defined when the size of a crack in the specimen reaches a size of around 1 mm, which can be visualized by human eyes and common cameras during the experiments. To accurately capture the instants at crack initiation, the current appearance of the specimen surfaces was compared with the initial one by digital photos during the tests. Due to difficulties in observing the cracks initiating inside the connections, crack initiation is defined by the first surface crack exceeding a length of about 1 mm at the surfaces of the specimens in this paper, where the crack length is illustrated in Fig. 5. This definition may overestimate the number of cycles at instant of crack initiation, while numerical simulation using proper cyclic plasticity models (e.g., Jia and Kuwamura 2013a) and micro-mechanism based fracture models (e.g., Jia and Kuwamura 2013b), may compensate this limitation and give a more accurate evaluation of crack initiation in future studies.

3.2 Hysteretic curves

Non-dimensionalized lateral load-lateral displacement curves and the corresponding skeleton curves of the specimens are shown in Fig. 6, where the instants at crack initiation of each specimen are also marked in the curves. The comparison results indicate that there is little difference among the hysteretic curves and the skeleton curves of the three specimens before crack initiation. Both the ultimate loads and the initial stiffnesses of the connections are similar to each other. Therefore, the post weld treatment has little effect on the global behaviors of the connections before crack initiation. However, the decrease in the loads of the two specimens with

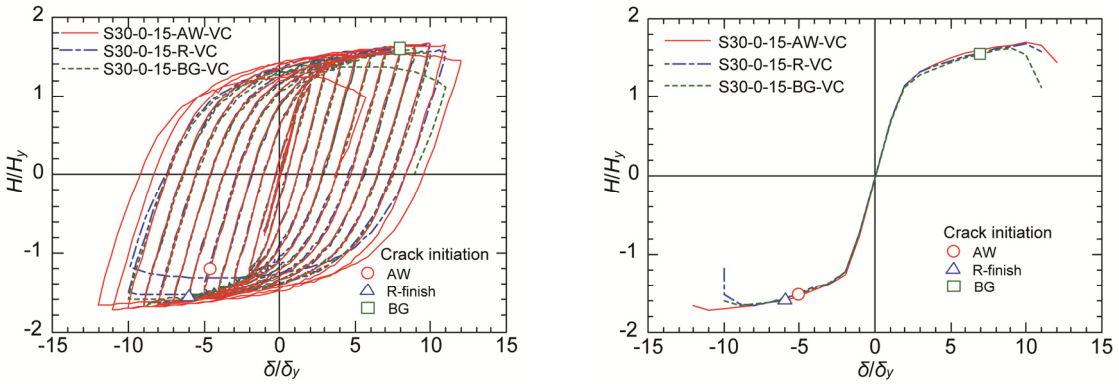

(a) Comparison of hysteretic curves (b) Comparison of skeleton curves

Fig. 6 Comparison of hysteretic curves and skeleton curves

weld finishes is faster than the as-welded one.

3.3 Failure modes

Different cracking modes as illustrated in Figs. 7 to 9, i.e., Mode 1: ductile crack initiated at the end of the weld bead of the beam-flange-to-beam-web joint, and Mode 2: ductile crack initiated at beam web edge close to the end of the fillet at the beam-web-to-column-web joint, were observed in the experiments, where the as-welded specimen failed in Mode 1, and the other two specimens failed in Mode 2. The crack initiated at the weld bead for Mode 1, while the crack initiated at the base metal for Mode 2. The locations and instants of the crack initiation are listed in Table 4, where the locations of the crack initiation are described by the height from the surface of the column flange. Herein, the failure processes of the specimens are detailed as follows

(1) Specimen S30-0-15-AW-VC

(i) $6\delta_y$ to $-6\delta_y$ within 12th half cycle: Crack initiation at the end of the weld bead of the beam-flange-to-beam-web joint as illustrated in Fig. 7(b) at Corner 1, was observed at this instant. The crack is located at 11 mm away from the surface of the column flange. The crack length, L_c, at this moment was 3.2 mm.

(ii) $7\delta_y$ within 14th half cycle: Another crack initiated along a discontinuous line at the end of the weld of the beam-flange-to-beam-web joint at Corner 2 as shown in Fig. 7(c). The crack length at the moment was 8.8 mm.

(iii) $9\delta_y$ within 18th half cycle: The crack at Corner 2 was propagating into the base metal of the beam flange as shown in Fig. 7(d), and the length of the crack was 18.8 mm. It was inferred that the crack had already run through the thickness of the weld.

(iv) $12\delta_y$ within 24th half cycle: The crack propagated into the beam flange along a diagonal direction, and the crack length was 60.1 mm at the moment as shown in Fig. 7(e). The crack also propagated into the beam web, and crack propagation became fast.

(v) $-12\delta_y$ within 25th half cycle: The crack has propagated into both the beam flange and beam web with large crack lengths as shown in Fig. 7(f). The crack length at the flange was 63 mm, where the test was terminated due to remarkable decrease in the lateral loads.

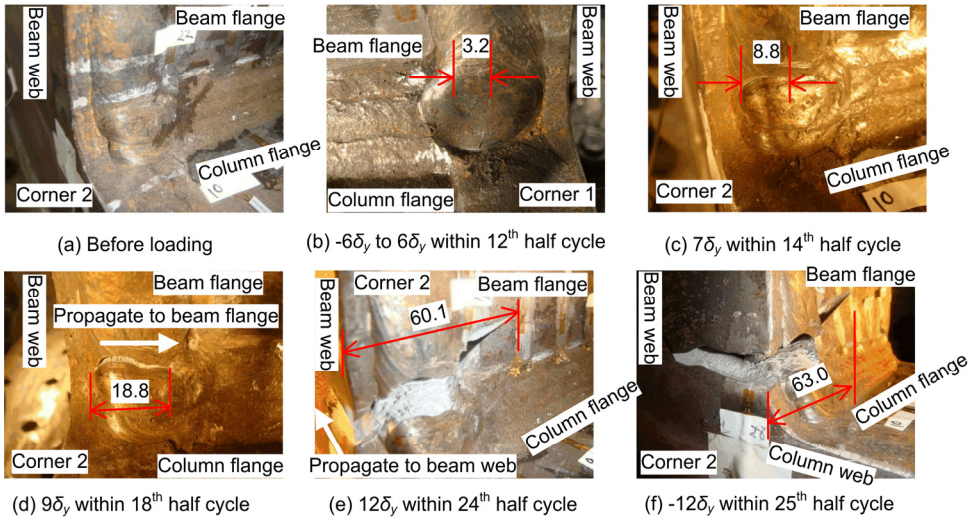

Fig. 7 Crack initiation and propagation of S30-0-15-AW-VC

Table 4 Instants and locations of crack initiation

Specimens	Instants at crack initiation	Locations of crack initiation (height from the column surfaces)
S30-0-15-AW-VC	11th half cycle (6δ_y to -6δ_y)	13
S30-0-15-R-VC	14th half cycle (-7δ_y)	11
S30-0-15-BG-VC	15th half cycle (8δ_y)	17

(2) Specimen S30-0-15-R-VC

(i) 7δ_y to -7δ_y within 15th half cycle: Crack initiating at the end of the fillet of the beam-web-to-column-web joint at Corner 1 was confirmed as shown in Fig. 8(b). The crack initiated at the base metal but not the welds, and the crack length at the moment was 3.3 mm. The R-finish treatment of the welds successfully transited the cracking at the weld beads to the base metal.

(ii) -8δ_y within 17th half cycle: The crack gradually propagated at the beam flange, and also tended to propagate into the beam web. The crack length at the moment was 5.9 mm. Besides, a new crack initiated close to the strain gauge at the beam flange as shown in Fig. 8(c).

(iii) -9δ_y within 19th half cycle: The first crack went on propagating at the beam flange, and tends to connect with the second crack as shown in Fig. 8(d). The length of the first crack at the moment was 33.6 mm. The crack also started to propagate into the beam web at -8δ_y within 19th half cycle.

(iv) -10δ_y within 21st half cycle: The crack propagated at both the beam flange and beam web as shown in Fig. 8(e), where the crack length at the beam flange was 43.5 mm.

(v) -11δ_y within 23rd half cycle: The crack length at the beam flange reached over half width of the flange, and it also propagated into the beam web with a considerable size as shown in Fig. 8(f), where the crack length was 92.3 mm at the beam flange. The propagation

along the beam web resulted in considerable decrease of the load-carrying capacity, and the experiment was terminated.

(3) Specimen S30-0-15-BG-VC

(i) $13\delta_y$ within 8th half cycle: At the moment, there was no crack initiating at the surfaces of the specimen. A marking line at the end of the fillet of the beam flange as shown in Fig. 9(b) to facilitate the identification of the pasting locations of the strain gauges can be observed, which is apt to be misunderstood as a crack during the tests.

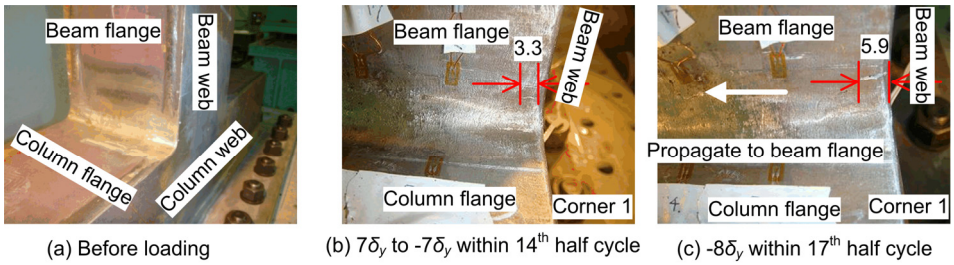

(a) Before loading (b) $7\delta_y$ to $-7\delta_y$ within 14th half cycle (c) $-8\delta_y$ within 17th half cycle

(d) $-9\delta_y$ within 19th half cycle (e) $-10\delta_y$ within 21st half cycle (f) $-11\delta_y$ within 23rd half cycle

Fig. 8 Crack initiation and propagation of S30-0-15-R-VC

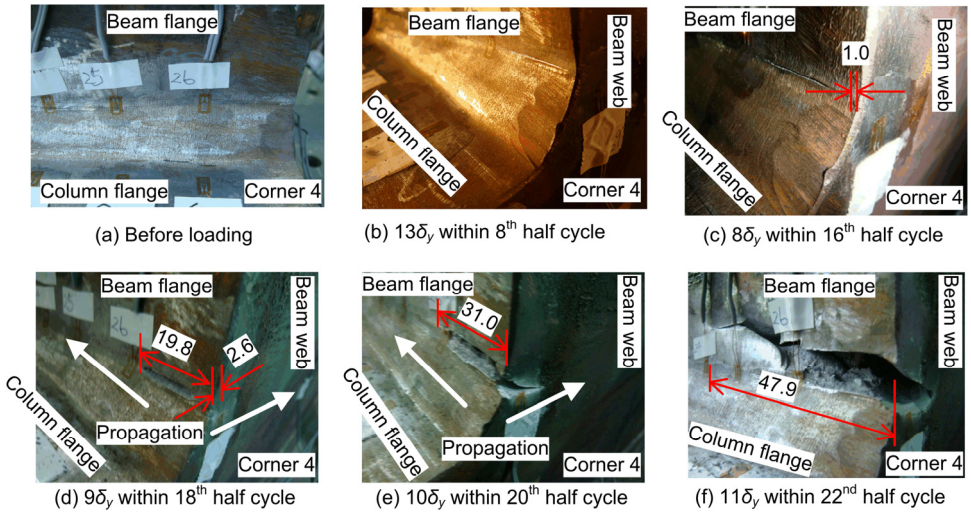

(a) Before loading (b) $13\delta_y$ within 8th half cycle (c) $8\delta_y$ within 16th half cycle

(d) $9\delta_y$ within 18th half cycle (e) $10\delta_y$ within 20th half cycle (f) $11\delta_y$ within 22nd half cycle

Fig. 9 Crack initiation and propagation of S30-0-15-BG-VC

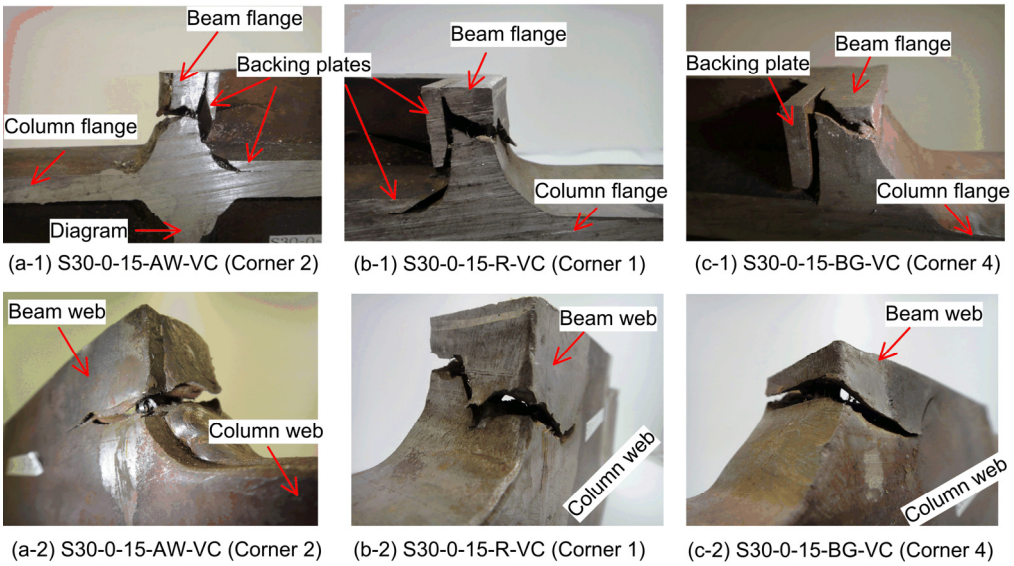

Fig. 10 Section view of cracks after cutting the specimens

(ii) $8\delta_y$ within 16th half cycle: A crack initiating at the end of the fillet at the beam-web-to-column-web joint was observed at Corner 4 of the specimen with a length of 1mm as shown in Fig. 9(c). The thickness of the marking line also became larger.

(iii) $9\delta_y$ within 18th half cycle: The crack propagated at both the beam flange and the beam web as shown in Fig. 9(d), and the crack lengths at the beam flange and beam web were 19.8 mm and 2.6 mm respectively. Compared with the as-welded specimen, the instants at crack propagation at the beam webs were earlier than the ones with weld finishes, which thus results in an earlier decrease in the lateral loads.

(iv) $10\delta_y$ within 20th half cycle: The crack propagated at both the beam flange and beam web as shown in Fig. 9(e), where the crack length at the beam flange was 31 mm.

(v) $11\delta_y$ within 22nd half cycle: The crack length at the beam flange reached 47.0 mm as shown in Fig. 9(f). The propagation at the beam flange and the beam web resulted in considerable decrease of the load-carrying capacity, and the experiment was terminated.

To observe the crack propagation at the internal of the specimens, the three specimens were cut after the tests. The section view of the cracks is given in Fig. 10, where the two backing plates at the beam-flange-to-beam-web joint and the beam-web-to-column-flange joint can be observed. The joints at the backing plates were welded first during the manufacturing, then the other plates were welded. Moreover, the ends of the two backing plates were tapered to avoid weld intersection at the beam-flange-to-column-flange joints. Since the crack initiation is at the beam-flange-to-web-flange joint, the effect of backing plate is minor in this study. The figure indicated that cracks initiated at the weld surfaces, and then propagated into the thickness of the welds or the beam flanges.

3.4 Comparison of crack initiation and propagation

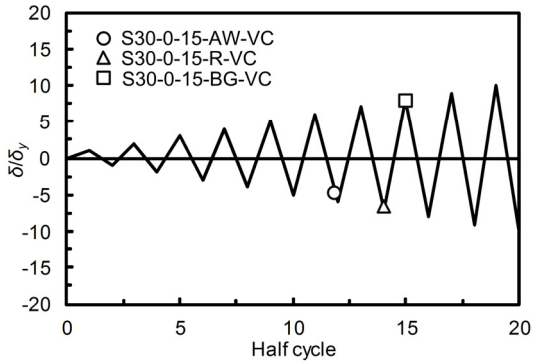

Fig. 11 Instants of crack initiation

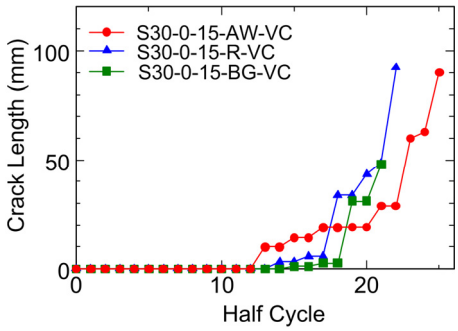

Fig. 12 Crack propagation of the specimens

The instants and locations of the crack initiation in the experiments are given in Table 4 and Fig. 11. Comparison among the test results indicates that the crack initiation at the as-welded specimen is the earliest, and the one with BG finish is the latest. Crack initiation instants of the specimens with R-finish and BG are respectively three and four half cycles later than the as-welded one, which implies that post weld treatment can significantly improve the ductile crack initiation lives of the beam-column connections. Meanwhile, apparent difference between the effects of the two finish methods, i.e., R-finish and BG, was not found in the tested specimens.

Crack propagation of all the specimens is compared based on the measured crack length illustrated in Fig. 12. The figure implies that the crack propagation of the specimens with post weld treatments is slower than the as-welded one within the first four half cycles after crack initiation, while faster after five half cycles. The instant at loss of load-carrying capacity of the as-welded specimen is later than the ones with post weld treatment, which is mainly due to the premature crack propagation in the beam webs for the specimens with weld finishes. Likewise, there is no apparent difference between the crack propagation behaviors of the two specimens with weld finishes.

3.5 Reduction of strain concentration effect for post weld treatment

To study the effect of post weld treatments on reducing strain concentration effect, strain gauges with large plastic strain measuring capacity, YFLA-2, were employed and pasted at the flanges and webs of both the beams and the columns, and the details are given in Fig. 13. The strain data versus half cycles curves at the four corners of the beam flanges (Gauges 1, 5 and 2, 6), at the mid-width of the beam flanges (Gauges 3, 7), and those at the corners of the beam-web-to-column-web joints (Gauges 4, 8), are all plotted in Fig. 14, where the instants of crack initiation are also marked in the curves. The comparison results at the four corners of the beam flanges indicate that the strain in the as-welded specimen is about 1 to 2% higher than the corresponding data of the ones with weld finishes, which can be found in Figs. 14(a) and (b). Fig. 14(c) implies that the strain at the mid-width of the beam flange is about two times of the corresponding data of the ones with weld finishes, and there is no apparent difference between the strain data of the two specimens with different weld finishes. Besides, no apparent difference is found among the strain data at the beam-web-to-column-web joints for all the specimens, which is found in Fig. 14(d). It is also interesting to find that the strain data at the beam-web-to-column-web joints are larger than

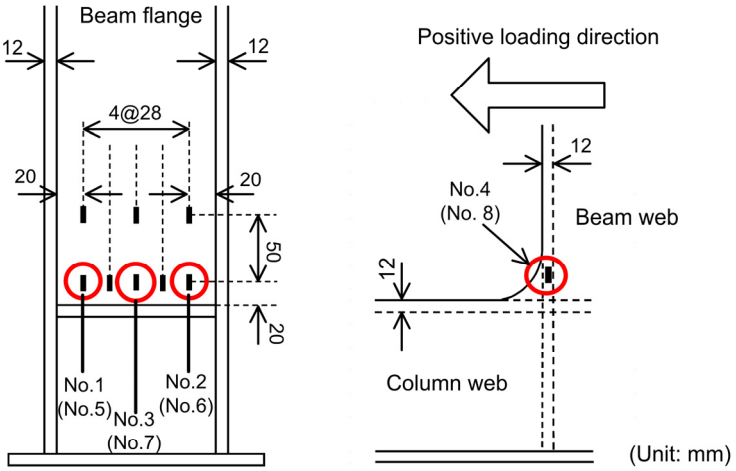

Note: the numbers in the brackets denote the corresponding strain gauge numbers in the symmetric locations.

Fig. 13 Arrangement of strain gauges

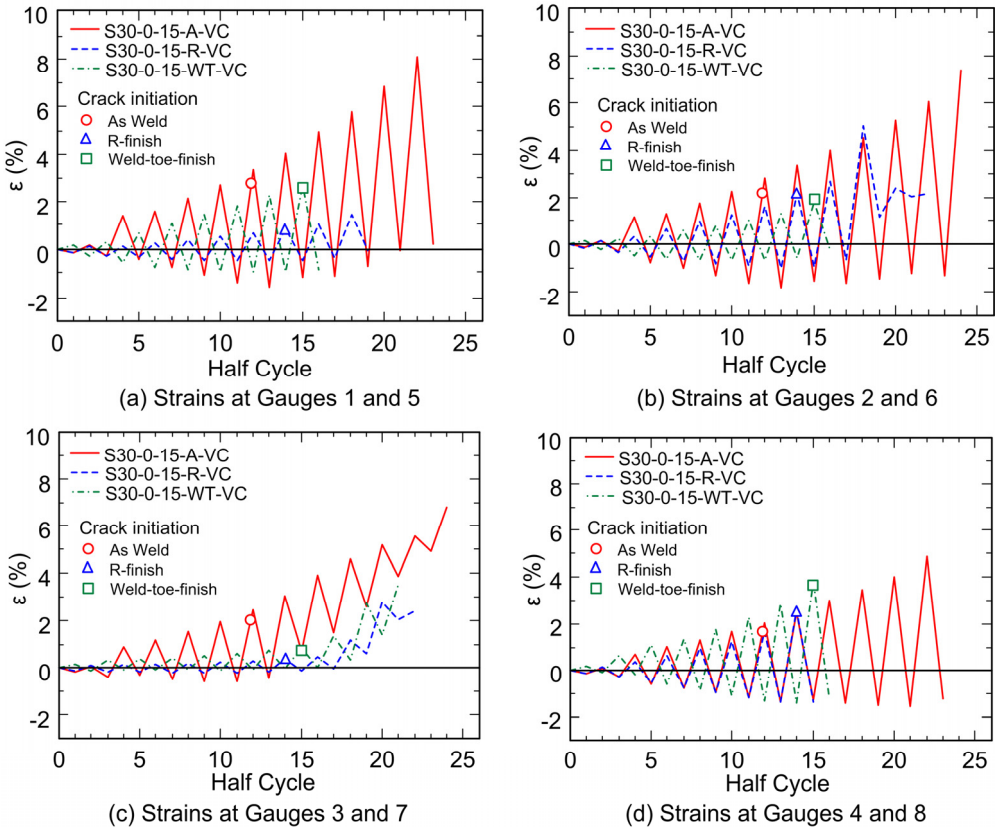

(a) Strains at Gauges 1 and 5

(b) Strains at Gauges 2 and 6

(c) Strains at Gauges 3 and 7

(d) Strains at Gauges 4 and 8

Fig. 14 Comparison of strain data

those at the beam flanges for the specimens with weld finishes, while an opposite conclusion is found for the as-welded specimen. Based on the aforementioned discussions, it is found that the post weld treatments can effectively reduce the strain concentration effect at the beam flanges, while they have minor effects on the strain concentration at the beam-web-to-column-web joints. Since the beam flanges were found to crack first, the post weld treatments can improve the crack initiation life of the welded connections.

4. Conclusions

In this study, experiments on three welded steel beam-column connections were carried out to study cracking behaviors of beam-column connections with different post weld treatments in welded steel moment-resisting frame bridge piers, where commonly full penetration welding is employed. The connections were tested under incremental loading with large displacement loading cycles to simulate the cracking behaviors during a strong earthquake event. The following conclusions can be drawn based on the experimental results carried out in this study.

- The two post weld treatment methods, i.e., R-finish, and burr grinding, can effectively delay the cracking initiation lives of the welded beam-column connections.
- The locations of crack initiation can be changed by the post weld treatments. A crack initiated at the discontinuous part at the weld bead of the as-welded specimen, while initiated at the ends of the fillets at the beam-web-to-column-web joints for the ones with post weld treatments.
- The crack propagation of the as-welded specimen is faster than the ones with post weld treatments at the early stage, while slower several half cycles later after the crack initiation.
- There is no apparent difference among the global load-displacement curves of all the specimens before crack initiation. The decrease in the loads is earlier for the specimens with post weld treatment due to earlier crack propagation at the beam webs compared with the as-welded one.
- The two post weld treatment methods can effectively reduce the strain concentration effect at the beam flanges, while have minor effects on the strain concentration at the beam-web-to-column-web joints.

Though great cautions were paid to the manufacturing process to simulate the actual conditions of the beam-column connections in steel bridge piers, it was still difficult to ensure the same details due to the limitations of the small-scaled specimens. Two backing plates were employed in the experiments due to requirements of the welding workmanship. Therefore, it is necessary to carry out full-scaled experiments with the same details as the practice to further validate the effects of post weld treatments on the cracking behaviors of the connections in future. Moreover, more experimental data are required to study the uncertainty in the experimental results due to inevitable deviations during manufacturing and testing.

Acknowledgments

The study is supported in part by grants from the JSPS Grants-in-Aid for Scientific Research (C) (No. 24560588), and the Advanced Research Center for Natural Disaster Risk Reduction,

Meijo University, which is supported by Ministry of Education, Culture, Sports, Science and Technology (MEXT), Japan.

References

American Welding Society D1.1 (1996), *Structural Welding Code-Steel*, Miami, FL, USA.

Architectural Institute of Japan (AIJ) (1995), *Fracture in Steel Structures during a Severe Earthquake*, Tokyo, Japan. [In Japanese]

Bruneau, M., Wilson, J.C. and Tremblay, R. (1996), "Performance of steel bridges during the 1995 Hyogo-ken Nanbu (Kobe, Japan) earthquake", *Can. J. Civ. Eng.*, **23**(3), 678-713.

EI-Tawil, S., Mikesell, T. and Kunnath, S.K. (2000), "Effect of local details and yield ratio on behavior of FR steel connections", *J. Struct. Eng., ASCE*, **126**(1), 79-87.

FEMA-350 (2000), Federal Emergency Management Agency (FEMA): Recommended seismic design criteria for new steel moment-frame buildings, Washington, D.C., USA.

Ge, H.B. and Kang, L. (2012), "A damage index-based evaluation method for predicting the ductile crack initiation in steel structures", *J. Earthq. Eng.*, **16**(5), 623-643.

Ge, H.B., Kang, L. and Tsumura, Y. (2013), "Extremely low-cycle fatigue tests of thick-walled steel bridge piers", *J. Bridge Eng., ASCE*, **18**(9), 858-870.

Ge, H.B. and Luo, X.Q. (2011), "A seismic performance evaluation method for steel structures against local buckling and extra-low cycle fatigue", *J. Earthq. Tsunami*, **5**(1), 1-17.

Haagensen, P.J. and Maddox, S.J. (2001), *IIW Recommendations on Post Weld Improvement of Steel and Aluminium*, IIW Doc. XIII-1815-00.

Iwashita, T. and Azuma, K. (2012), "Effect of plastic constraint on brittle fracture in steel: evaluation using a toughness scaling model", *J. Struct. Eng., ASCE*, **138**(6), 744-752.

Jia, L.J. and Kuwamura, H. (2013a), "Prediction of cyclic behaviors of mild steel at large plastic strain using coupon test results", *J. Struct. Eng., ASCE*, **140**(2), 04013056.
DOI: 10.1061/(ASCE)ST.1943-541X.0000848

Jia, L.J. and Kuwamura, H. (2013b), "Ductile fracture simulation of structural steels under monotonic tension", *J. Struct. Eng., ASCE*, **140**(5), 04013115.
DOI: 10.1061/(ASCE)ST.1943-541X.0000944

Kang, L. and Ge, H.B. (2013), "Predicting ductile crack initiation of steel bridge structures due to extremely low-cycle fatigue using local and non-local models", *J. Earthq. Eng.*, **17**(3), 323-349.

Kirkhope, K.J., Bell, R., Caron, L., Basu, R.I. and Ma, K.T. (1999a), "Weld detail fatigue life improvement techniques. Part 1: review", *Mar. Struct.*, **12**(6), 447-474.

Kirkhope, K.J., Bell, R., Caron, L., Basu, R.I. and Ma, K.T. (1999b), "Weld detail fatigue life improvement techniques. Part 2: application to ship structures", *Mar. Struct.*, **12**(7-8), 477-496.

Kuwamura, H. (1997), "Transition between fatigue and ductile fracture in steel", *J. Struct. Eng., ASCE*, **123**(7), 864-870.

Kuwamura, H. (2003), "Classification of material and welding in fracture consideration of seismic steel frames", *Eng. Struct.*, **25**(5), 547-563.

Kuwamura, H. and Yamamoto, K. (1997), "Ductile crack as trigger of brittle fracture in steel", *J. Struct. Eng., ASCE*, **123**(6), 729-735.

Kuwamura, H., Iyama, J. and Matsui, K. (2003), "Effects of material toughness and plate thickness on brittle fracture of steel members", *J. Struct. Eng., ASCE*, **129**(11), 1475-1483.

Kuwamura Lab. (1995), *Field Survey Report on Structural Damage during the 1995 Hyogoken-Nanbu Earthquake*, School of Engineering, The University of Tokyo, Tokyo, Japan. [In Japanese]

Luo, X.Q., Ge, H.B. and Ohashi, M. (2012), "Experimental study on ductile crack initiation in compact section steel columns", *Steel Compos. Struct., Int. J.*, **13**(4), 383-396.

Mahin, S.A. (1998), "Lessons from damage to steel buildings during the Northridge earthquake", *Eng.*

Struct., **20**(4-6), 261-270.
Mao, C., Ricles, J., Lu, L.W. and Fisher, J. (2001), "Effect of local details on ductility of welded moment connections", *J. Struct. Eng*., *ASCE*, **127**(9), 1036-1044.
Mashiri, F.R., Zhao, X.L. and Grundy, P. (2001), "Effects of weld profile and undercut on fatigue crack propagation life of thin-walled cruciform joint", *Thin-Wall. Struct*., **39**(3), 261-285.
Metropolitan Expressway Company Limited (2008), *Recommendations for the Design and Construction of Bridges*, Tokyo, Japan. [In Japanese]
Miki, C. and Sasaki, E. (2005), "Fracture in steel bridge piers due to earthquakes", *Int. J. Steel Struct*., **5**(2), 133-140.
Nagoya Expressway Public Corporation (2004), *Standard Atlas for Steel Structures*, Nagoya, Japan. [In Japanese]
Nakashima, M., Inoue, K. and Tada, M. (1998), "Classification of damage to steel buildings observed in the 1995 Hyogoken-Nanbu earthquake", *Eng. Struct*., **20**(4-6), 271-281.
O'Sullivan, D., Hajjar, J. and Leon, R. (1998), "Repairs to mid-rise steel frame damaged in northridge earthquake", *J. Perform. Constr. Facil*., *ASCE*, **12**(4), 213-220.
Pedersen, M., Mouritsen, O., Hansen, M., Andersen, J. and Wenderby, J. (2010), "Comparison of post-weld treatment of high-strength steel welded joints in medium cycle fatigue", *Welding in the World*, **54**(7-8), R208-R217.
Qian, X., Choo, Y., Liew, J. and Wardenier, J. (2005), "Simulation of ductile fracture of circular hollow section joints using the gurson model", *J. Struct. Eng*., *ASCE*, **131**(5), 768-780.
Qian, X., Petchdemaneengam, Y., Swaddiwudhipong, S., Marshall, P., Ou, Z. and Nguyen, C.T. (2013), "Fatigue performance of tubular X-joints with PJP+ welds: I — Experimental study", *J. Constr. Steel Res*., **90**(11), 49-59.
Ricles, J., Mao, C., Lu, L.W. and Fisher, J. (2002), "Inelastic cyclic testing of welded unreinforced moment connections", *J. Struct. Eng*., *ASCE*, **128**(4), 429-440.
Roeder, C.W., Lehman, D.E. and Yoo, J.H. (2005), "Improved seismic design of steel frame connections", *Int. J. Steel Strut*., **5**(2), 141-153.
Schafer, B.W., Ojdrovic, R.P. and Zarghamee, M.S. (2000), "Triaxiality and fracture of steel moment connections", *J. Struct. Eng*., *ASCE*, **126**(10), 1131-1139.
Stojadinović, B., Goel, S.C., Lee, K.H. and Choi, J.H. (2000), "Parametric tests on unreinforced steel moment connections", *J. Struct. Eng*., *ASCE*, **126**(1), 40-49.
The Building Center of Japan (2003), *Guidelines for Prevention of Brittle Fracture at the Beam Ends of Welded Beam-to-column Connections in Steel Frames*, Tokyo, Japan. [In Japanese]
Usami, T. and Ge, H.B. (2009), "A performance-based seismic design methodology for steel bridge systems", *J. Earthq. Tsunami*, **3**(3), 175-193.

BU

Nomenclature

B	flange width of beam and column
D	web width of beam
E	Young's modulus
E_{st}	initial strain hardening modulus
H_y	yield strength of lateral load
L	beam length
L_c	crack length
R	curvature radius of fillet
R_f	width-to-thickness parameter
a	incomplete penetration depth
b	width of beam flange
h	column height
hc	web width of column
N	number of sub-panels
R	radius of gyration of beam section
T	thickness of beam flange
δ	horizontal displacement at beam end
δ_y	initial yield displacement
ε	strain
ε_f	uniform strain at fracture
ε_{st}	strain at initiation of strain hardening
ε_u	yield strain
$\bar{\lambda}$	slenderness ratio parameter
v	Poisson's ratio
σ_u	tensile strength
σ_y	initial yield stress